ISSN 0027-1349, Moscow University Physics Bulletin, 2015, Vol. 70, No. 4, pp. 303–311. © Allerton Press, Inc., 2015.
Original Russian Text © E.A. Kiseleva, V.O. Mikhailov, E.I. Smolyaninova, E.P. Timoshkina, P.N. Dmitriev, 2015, published in Vestnik Moskovskogo Universiteta. Fizika, 2015, No. 4, pp. 87–94.

PHYSICS OF EARTH, ATMOSPHERE, AND HYDROSPHERE

The Combination of Methods for Analyzing the Amplitude and Phase of Satellite Radar Images for the Estimation of Displacements on Landslide-Affected Slopes

E. A. Kiseleva[a], V. O. Mikhailov[a, b], E. I. Smolyaninova[a], E. P. Timoshkina[a], and P. N. Dmitriev[a]

[a] *Schmidt Institute of Physics of the Earth, Russian Academy of Sciences, ul. B. Gruzinskaya 10, Moscow, 123995 Russia*
e-mail: e.kiseleva@ifz.ru, mikh@ifz.ru

[b] *Department of Physics, Moscow State University, Moscow, 119991 Russia*

Received March 3, 2015; in final form, April 12, 2015

Abstract—The efficiency of combining methods for analyzing the amplitude and phase of radar images from the ENVISAT, ALOS, and TerraSAR-X satellites is shown based on a case study of a landslide in Baranovka Settlement, Greater Sochi. The offset tracking method in the amplitude field of the reflected radar signal allowed us to define the contour of the area where the landslide occurred in the night between January 23 and 24, 2012 and to estimate the displacements in different parts of the landslide body. The maximum displacement was 7.5 ± 1 m. The displacements prior to the landslide from January 22, 2007 until September 17, 2010, as obtained from the ALOS satellite by the persistent scatterer method, demonstrate seasonal autumn–winter accelerations. The time series of displacements from the ENVISAT satellite shows that from November 29, 2010 until July 27, 2011 the displacement rates in the line-of-sight direction v_{LOS} were relatively small (21 mm/yr), but in the period from September 25, 2011 to December 24, 2011 the slide rate increased to 50 mm/yr. As obtained by the TerraSAR-X satellite, the slide rate v_{LOS} after landsliding in the period from February 17, 2012 to March 10, 2012, reached 30 mm/month, but after June 6, 2012 it decelerated to 2–3 mm/month. Similar slide rates were also obtained for the same periods based on differential interferograms.

Keywords: satellite radar interferometry, landslides, monitoring.

DOI: 10.3103/S0027134915040116

INTRODUCTION

Synthetic aperture radar (SAR) is widely applied for remote sensing of the Earth, because radar images can be made for any illumination and level of cloudiness. The most important civil-purpose problems that are related to SAR application are the construction of digital elevation maps (DEMs) and the monitoring of displacements for natural and technogenic objects.

A radar image is a matrix of complex numbers that characterize the amplitude and phase of a radar signal from some resolution site (pixel). For the estimation of displacements, a differential interferogram is usually calculated, viz., the difference between the phases of radar signals that are reflected from the same pixel during the first and second imaging, minus a correction for the change in form during the second imaging (a DEM is required). After filtering of the atmosphere effects and eliminating the errors of set orbits and the DEM, we obtain the phase difference that is caused by the reflecting site displacement for the time between repeated signals in the line-of-sight (LOS) direction, plus different noises and errors. It is important that the field of phase displacements is convoluted on the 2π modulus and phase unwrapping is necessary to obtain the displacements in length units. Analysis of differential interferograms (DInSAR; differential interferometry) allows researchers to study coseismic slips, landslide displacements, glacier dynamics, magmatic intrusions, and other processes that cause phase-displacement fields that are discernible on the noise background (some results of Russian research were given in [1–3]). In addition to different noises, application of the DInSAR method to slow processes (displacements above tunnels, mines, and in the areas of oil and gas recovery) is limited by the necessity of using the images that are made with a long time interval in order to accumulate sufficient displacement values. However, if the time intervals are a year or more, temporal decorrelation takes place between the images due to landscape changes and other processes.

Considerable advances have been achieved in the recent 15 years due to the development of persistent scatterer (PS) methods: these methods use analysis of a differential interferogram series that reveals particular pixels that show stable reflection of a radar signal. Then, from the time series of each PS offset, the long-term trends are distinguished by filtering or by searching for signals of a set form (linear, periodic, etc); therefore, high-frequency noises are considerably eliminated and slow (a few mm per year) temporally

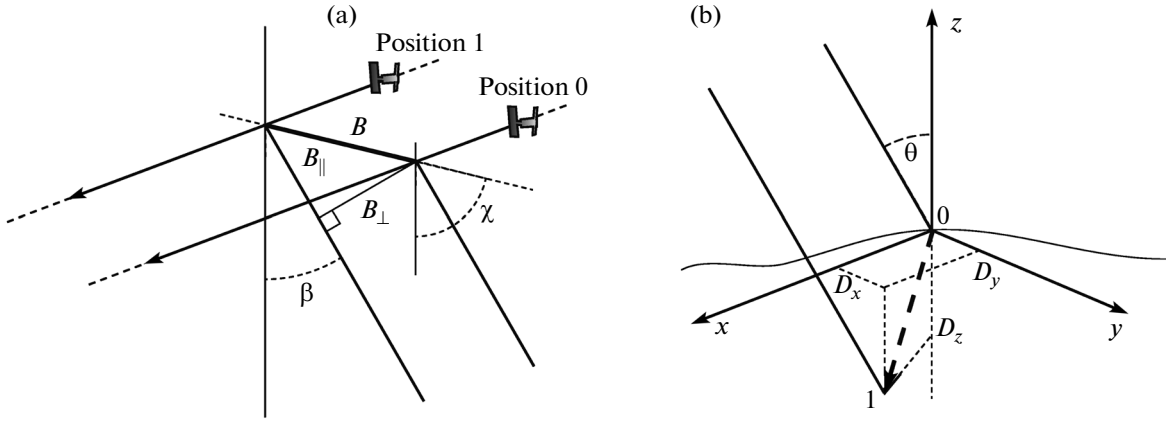

Fig. 1. The geometry of repeated imaging (a) and the coordinate system on the Earth's surface for estimating the full vector modulus of the displacement from point 0 to point 1 (b). Here, B is the base line, $B_{\|}$ and $B_{\perp}$ are parallel and perpendicular components of the base line; β is the angle of the satellite LOS; θ is the angle of radar-beam incidence; χ is the angle of the base line. The 0x axis is parallel to the direction of the satellite flight; the z0y plane coincides with the LOS plane; D_x, D_y, and D_z are the components of the offset vector for the time between two imaging dates.

persistent displacements can be detected. These methods are most effective when studying the displacements of technogenic objects with a high level of reflectivity [4]. Natural objects usually have a weaker level of reflectivity and a certain difficulty occurs in their detection on the background of noise signals. However, usually the characteristic dimensions of the areas with displacements of a natural origin are considerably greater than the pixel size (a pixel is no more than 20 m in size); thus, methods for detecting offset field components correlated in space and time were developed for natural objects. The method that was used in the present work is among these methods: it was proposed in [5] and implemented in the StaMPS software package [6]. The successful monitoring of natural objects largely depends on the appropriate choice of filter parameters and wavelength of SAR imaging. A detailed discussion on this point can be found, for example, in [7].

If there were considerable displacements (epicentral earthquake zone, rapid movements of glaciers, or landslides) in the period between sequential images, or if the images were made with a very long time interval, SAR interferometry becomes inapplicable because of full temporal decorrelation. For these cases, offset tracking methods for detecting offsets in the field of reflected signal amplitudes have been developed [8–11]. Offsets are calculated during image registration at the subpixel level both in the direction of satellite flight (azimuth) and in that perpendicular to the satellite orbit (ground range in [1]). The offset tracking method is often the only way to analyze considerable localized displacements.

The present paper combines all three of these methods of SAR-image analysis when studying the landslide processes. A case study of a landslide in Baranovka Settlement, in the Khosta distinct of Greater Sochi is considered. Below, a brief description of the offset tracking method will be given; then, we will consider the data on the SAR images, some general information about the landslide under study, and finally provide calculation results and their interpretation.

1. THE OFFSET TRACKING METHOD

One of the first stages of SAR image processing is the registration of a pair of images; this procedure also has several steps. First of all, an approximate (within the accuracy of tens of pixels) estimate of the offset for one image relative to another is calculated by using orbital ephemerides. For a more accurate fit, cross-correlation sliding window methods are used. The position of the maximum of the 2D cross correlation function yields the value of the offset between two images on both the ground range and the azimuth. In order to enhance the accuracy of offset estimation, interpolation to a lower-size mesh is used for the entire set of windows. As a result of this, well-correlated images can yield an accuracy of the offset estimate of up to 1/20th of a pixel, which corresponds to 20 cm on the azimuth and 1 m on the ground range for ENVISAT images [12]. In the case of detailed TerraSAR images, this value is 15 cm.

The offset values on the azimuth (d_a) and range (d_r) obtained from image registration are determined by both surface displacement between images (let us denote these parameters as δ_a and δ_r, respectively) and changes in the geometry of imaging (so-called orbital component of offsets). The orbital component depends on the base line value ($B_{\perp}$, Fig. 1) and on the angle between satellite flight directions that correspond to the first and second images. In order to take orbital offsets into account, we can use functions that are linear for the radar coordinates [9, 10]. The offsets

in the directions of the azimuth δ_a and range δ_r, which are free from the orbital component, can then be calculated by the following formulas:

$$\begin{aligned} \delta_a &= d_a - (a_0 + a_1 l + a_2 p), \\ \delta_r &= d_r - (b_0 + b_1 j + b_2 p), \end{aligned} \quad (1)$$

where l and p are the radar coordinates and a_0, a_1, a_2, b_0, b_1, and b_2 are the coefficients of the bilinear model that is used for the estimation of the orbital component of the offsets.

Thus, Eqs. (1) contain six unknown values: a_0, a_1, a_2, b_0, b_1, and b_2. To find them, we can use so-called reference points with known locations and offset values [10]. In practice, known objects that do not move, such as rock outcrops, are often used as reference points. The validity and accuracy of this method depends on the number of reference points and on how uniformly they are distributed over the area.

To estimate three components of the offset vector, let us apply the approach that was proposed in [8]. Let the considered point on a surface be the origin of a rectangular coordinate system where the x axis is the horizontal axis, which is parallel to the azimuth, the y axis is also horizontally oriented in the plane of the satellite's line-of-sight, and the z axis is oriented vertically (Fig. 1). Then we have

$$\begin{aligned} \delta_a &= D_x/S_a, \\ \delta_r &= (B\cos(\chi - \beta) + D_y \sin\theta - D_z \cos\theta)/S_r, \end{aligned} \quad (2)$$

where β is the angle of the satellite LOS; θ is the angle of incidence; χ is the base line angle; and S_a and S_r are the spatial resolutions (in meters) on the azimuth and range, respectively.

It is obvious that estimation of three components of the offset vector (D_x, D_y, and D_z) for the time $\Delta t = t_1 - t_0$ between two imaging episodes cannot be made solely on the basis of Eqs. (2). If images are made from both ascending and descending orbits for the considered area, another two equations that are analogous to (2) can be obtained. In these equations, the unknown will be the same three components of the offset vector and the values D_x, D_y, and D_z can be accurately estimated (see, for example, [11]). If only images that were made from one orbit are available, the problem solution requires that additional assumptions be introduced. It was taken in [8, 10] that the surface on which the landslide-affected rock volume moves conforms to the day surface. Displacements for the time, Δt, on the horizontal axes, D_x and D_y, and that on the vertical axis, D_z, are then connected via the following equation

$$D_z = D_x \frac{\partial}{\partial x} z(x, y) + D_y \frac{\partial}{\partial y} z(x, y),$$

where $z = z(x, y)$ is the DEM in x and y coordinates. If a_a and a_r are the angles of the relief inclination in the $x0z$ and $x0y$ planes, as calculated relative to the local horizontal line from the DEM, then any small offset on x and y corresponds to vertical slip

$$D_z = D_x \tan\alpha_a + D_y \tan\alpha_r. \quad (3)$$

We note that this assumption is inapplicable to the landslide base where moving material accumulates.

Now, we can estimate the modulus of the full offset vector:

$$D = \sqrt{D_x^2 + D_y^2 + D_z^2}. \quad (4)$$

It was shown in [13] that application of Eq. (3) to the data from two tracks for the landslide that occurred in the area of Kepsha village near the Adler–Krasnaya Polyana road yielded the direction of the landslide offset close to the direction of the maximum slope angle on the relief.

An advantage of the offset tracking methods compared to those of radar interferometry is that offsets are estimated immediately in length units, i.e., no additional phase unwrapping is necessary. At large offsets, when the displacements of the adjacent pixels exceed the half wavelength, unwrapping can cause errors. In addition, offset tracking allows the displacements to be estimated in both the LOS direction (the ground range, analogous to the SAR interferometry) and along the track (on the azimuth).

2. COMBINATION OF THE DINSAR, PSINSAR, AND OFFSET TRACKING METHODS: A CASE STUDY OF THE LANDSLIDE IN BARANOVKA SETTLEMENT, GREATER SOCHI

2.1. Satellite Data

We used three sets of images of the Baranovka Settlement area in the Khosta district of Sochi, where a large landslide occurred in the night between January 23 and 24, 2012. SAR images cover the interval from January 2007 until September 2012 without considerable time gaps. More precisely, 18 images (January 22, 2007–September 17, 2010) were made from the ascending orbit of the 588th track of the ALOS PALSAR satellite; 13 images (December 24, 2011–September 13, 2012) were made from the ascending orbit of the 35th track of the ENVISAT satellite, after orbital correction in October 2010; and 18 images (December 24, 2011–September 13, 2012) were made from the ascending orbit of the 54th track of the TerraSAR-X satellite. The flight direction and LOS of the satellites and the coverage of images are shown in Fig. 2a, while the imaging dates are in the timescale in Fig. 2b.

2.2. The Landslide in the Baranovka Settlement

This landslide is one of multiple landslide episodes in the surroundings of Greater Sochi. The last large displacements of this body occurred in 1988 and 2012. According to [14], the precipitation in the area of Sochi in the January 1–23, 2012 period was from 68 to

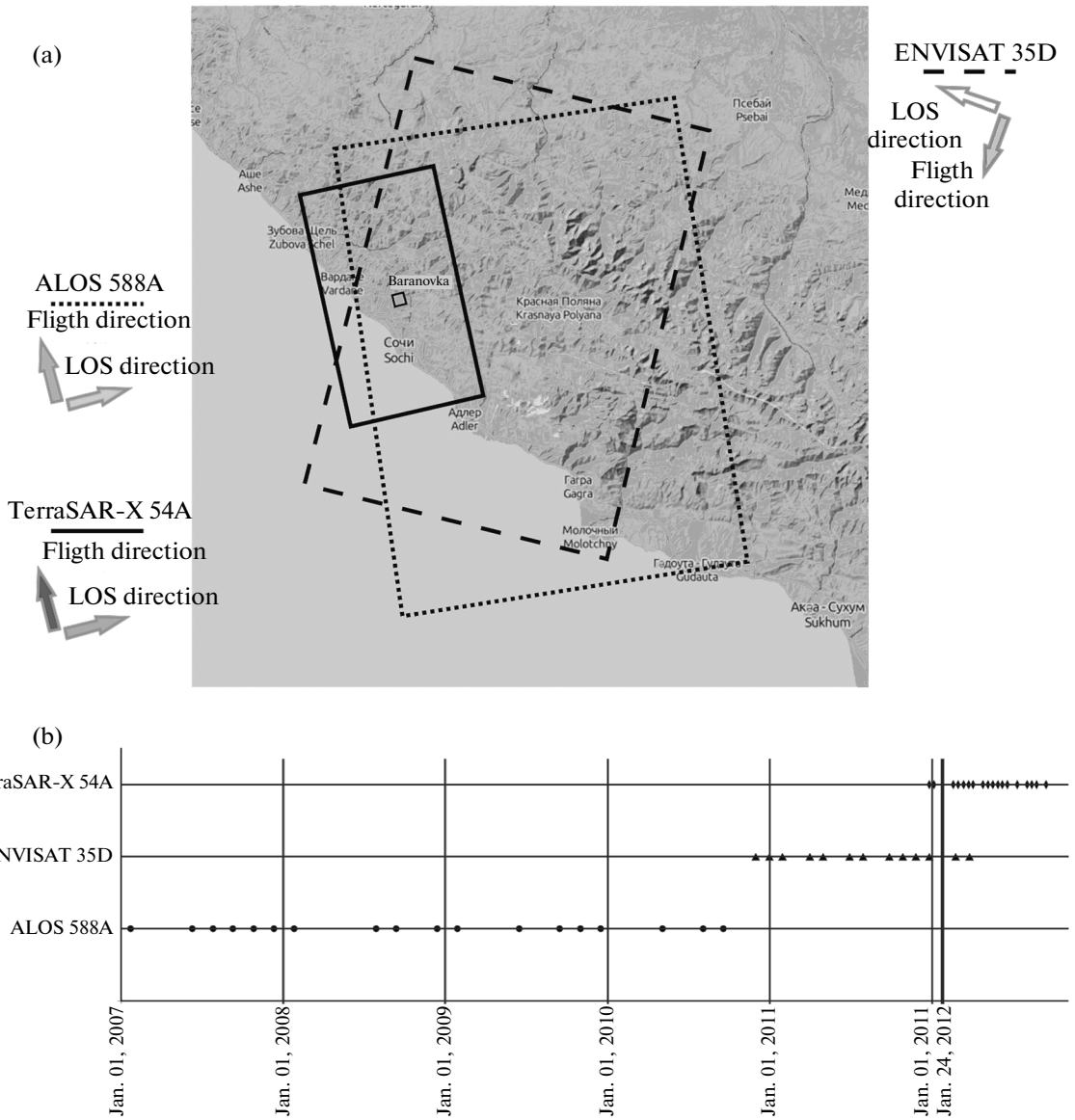

Fig. 2. Satellite data. (a) The contours of images in the Google Earth map. The satellite flight directions, LOS directions, and coverage of images are indicated. The white rectangle is the landslide area in Baranovka Settlement (b) Imaging dates. Dark circles denote ALOS images; dark triangles, ENVISAT; rhombuses, TerraSAR-X.

78 mm; this led to the overwetting of slopes and likely caused landslide activation. The most intensive displacements occurred in the eastern Baranovka Settlement. Fortunately, no human deaths were reported, but a special commission concluded that 35 private houses became unsuitable for dwelling (some of the houses were completely destroyed). As reported by eyewitnesses (local inhabitants), the landslide body activated as early as December 2011 when house walls cracked and pipes and windowpanes broke. Unfortunately, ground data on this landslide episode are scarce. Based on the data from a web site [15], investigation of the landslide-affected slope was carried out by the OOO Inzhzashchita. The length of the landslide body was 780 m, the width was 300–370 m, and the thickness was at least 20–30 m; the area of the landslide was 23.3 ha and its volume was estimated at 4.6 mil m^3. The landslide head was located at the escarpment of an ancient landslide basin on a forested slope at a 30°–35° angle. Below the detachment edge, cracks up to 10–15 cm wide with a depth of up to 0.5 m were observed; damage to road pavement and concrete walks, and deformation of houses were documented. In the middle part of the landslide body, multiple tension cracks widened up to 0.5 m; the heights of the secondary detachment edges increased to 1.5 m; complete destruction of the road pavement occurred, along with considerable deformation and destruction in near-house areas, as well as large (up to 15–20 cm) cracks in house and retaining walls. These

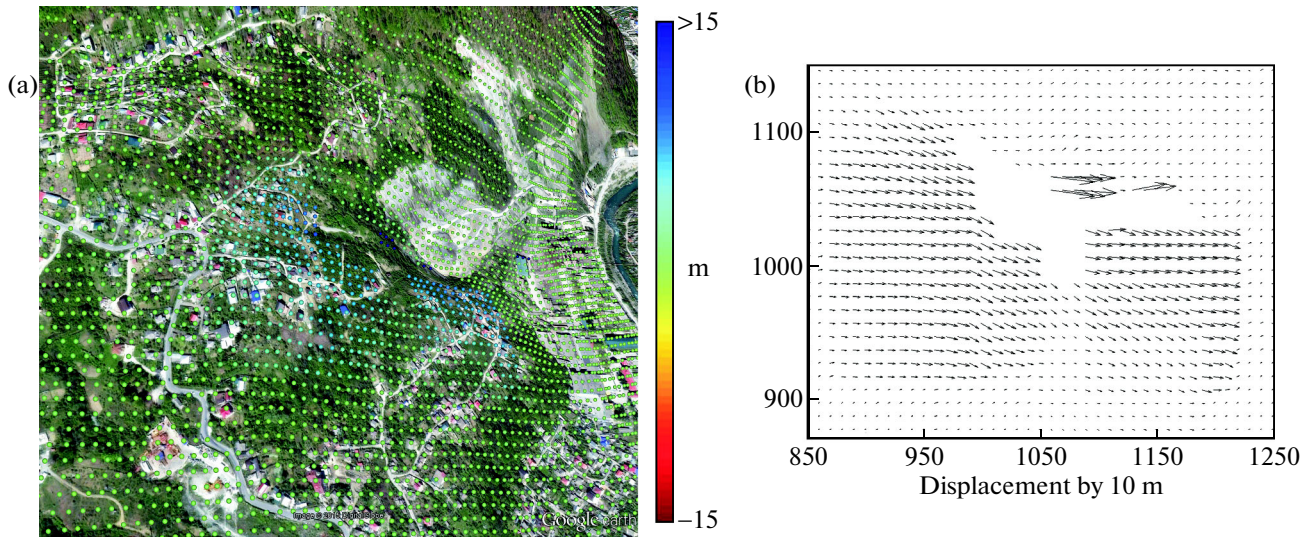

Fig. 3. The values of the offset vector modulus, D, in the period from January 4 until February 17, 2012 (toned) in the Google Earth map (a) and the direction of displacements as projected to the $x0y$ plane (b). The size of an arrow is proportional to the displacement value.

data, jointly with the analysis of photo images that were published in the Internet, suggest that the displacement length on the slope could be 5 m or more.

2.3. Results

First, the images from the ALOS PALSAR, ENVISAT, and TerraSAR-X satellites were sequentially analyzed using offset tracking. As expected, visible displacements were obtained on the pair of TerraSAR-X images that were nearest to the landslide episode in time: the image of January 4, 2012 (20 days before the landslide activation in the night between January 23 and 24) and that of February 17, 2012 (3 weeks after the landslide activation). The base line (B) between these images is 50.9 m. After accurate image registration, 22500 windows that are 32×32 pixels in size (azimuth vs. range) were chosen. In the centers of the chosen windows, the values of the D_x, D_y, and D_z displacements were calculated in accord with Eqs. (2) and (3) for the period from January 4 until February 17, 2012 and the values of the offset vector modulus, D, were estimated according to formula (4). After geocoding, the results were plotted on the map in Google Earth (Fig. 3a); the direction of the displacement in projection to the $x0y$ plane ($\tan^{-1}D_x/D_y$) is shown in Fig. 3b.

The values of the offset vector modulus, D, for the areas that are most affected by the landslide in the January 4–February 17, 2012 period are the following. In the northern part of Cherechnevyi per. (Fig. 4d), the total displacement in this period was approximately 6.4 ± 1 m; in the northern part of Kombinatskii per., approximately 7.5 ± 1 m; in the central part of Armyanskaya ul., near its crossing with the Chereshnevyi per., it was 5.1 ± 1 m. The zones of the maximum displacements that were distinguished by offset tracking coincide with those where the Commission for Emergency Prevention and Recovery of the Sochi Administration introduced an emergency regime on January 26, 2012.

Offset tracking did not yield the estimates of displacements from images that were made in the descending orbit of the 35th track of the ENVISAT satellite from December 24, 2011 until February 22, 2012. This is probably related to the base line size (475 m) between the orbits on December 24, 2011 and February 22, 2012; such a distance lowers the coherence to a level that is insufficient even for offset tracking.

Calculations were then made by the persistent scatterer method and with the StaMPS software for the images from the ALOS, ENVISAT, and TerraSAR-X satellites. In order to increase the number of obtained PSs in the landslide area and to avoid unwrapping errors due to the previously found considerable displacements in the period from January 23–24 until February 17, 2012, we used (a) 11 images from the ENVISAT satellite that were made in the December 29, 2010–December 24, 2011 period (i.e., all of the images that were made before the landslide activation) and (b) 16 images from the TerraSAR-X satellite that were made in the February 17–September 13, 2012 period (i.e., all of the images that were made after the landslide activation). The mean displacement rates in the sites of PS identification, in projection to the LOS (v_{LOS}) of ALOS, ENVISAT, and TerraSAR-X satellites, are shown in Figs. 4a–4c, as well as the landslide contours that were obtained by the offset tracking.

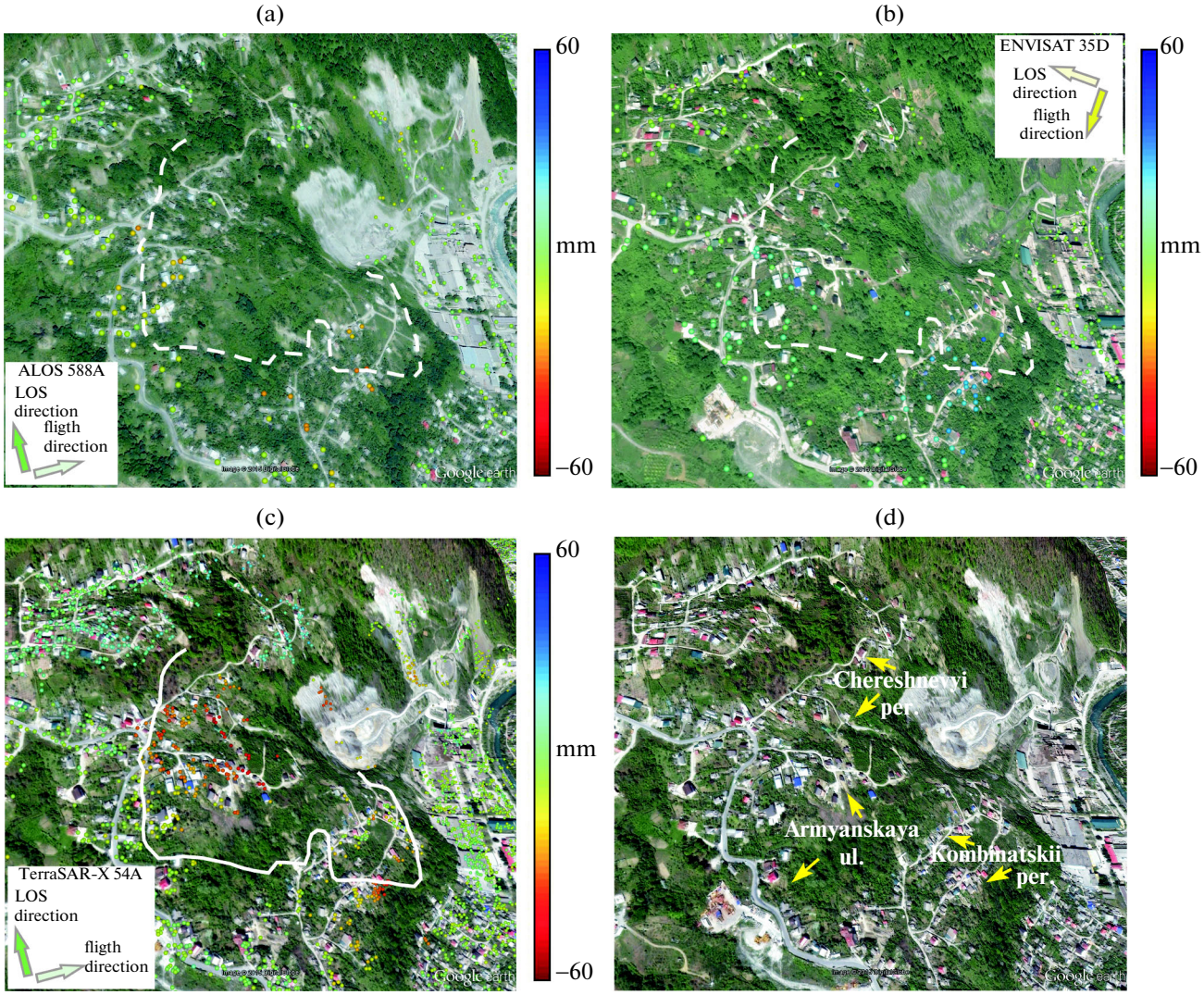

Fig. 4. The mean displacement rates v_{LOS} for persistent scatterers as obtained from ALOS (a), ENVISAT (b), and TerraSAR-X(c) images. The landslide outlines as revealed by offset tracking are drawn in a white dashed line in (a) and (b) and with a solid line in (c). (d) The locations of Armyanskaya st., Chereshnevyi per. and Kombinatovskii per. in the Google Earth map.

3. DISCUSSION

The results of data analysis from different satellites (Fig. 4) are overlain on Google Earth images from different times: September 27, 2009 for ALOS; September 27, 2009 for ENVISAT; and April 14, 2013 for TerraSAR-X. A thorough analysis of the images reveals the considerably denser buildings in the landslide-affected area. Intensive building together with the long-term heavy rain were apparently the main causes of the catastrophic event.

Despite the relatively small number of PSs that were identified within the landslide area during calculations from the ALOS and ENVISAT satellites data (Figs. 4a and 4b), displacements before the landslide activation (at least since January 22, 2007) have been clearly identified in the central part of Armyanskaya ul. and in the southern part of Kombinatovskii per. Based on the data from the ALOS satellite, the mean displacement rates v_{LOS} in the central part of Armyanskaya ul. were up to 16.3 mm/yr in the period from January 22, 2007 until September 17, 2010, while they were 10.7 mm/yr based on the data from the ENVISAT satellite in the November 29, 2010–March 23, 2012 period. The respective v_{LOS} values in the southern part of Kombinatovskii per. were 20 and 22.5 mm/yr.

Let us now consider the time series of displacements in the central part of Armyanskaya ul., near its crossing with Chereshnevyi per., which were obtained via persistent scatterers during the calculation on the bases of the images from ALOS, ENVISAT, and TerraSAR-X satellites (Fig. 5). As obtained by ALOS satellite from January 22, 2007 until September 17, 2010, in the time series of displacements in the LOS direc-

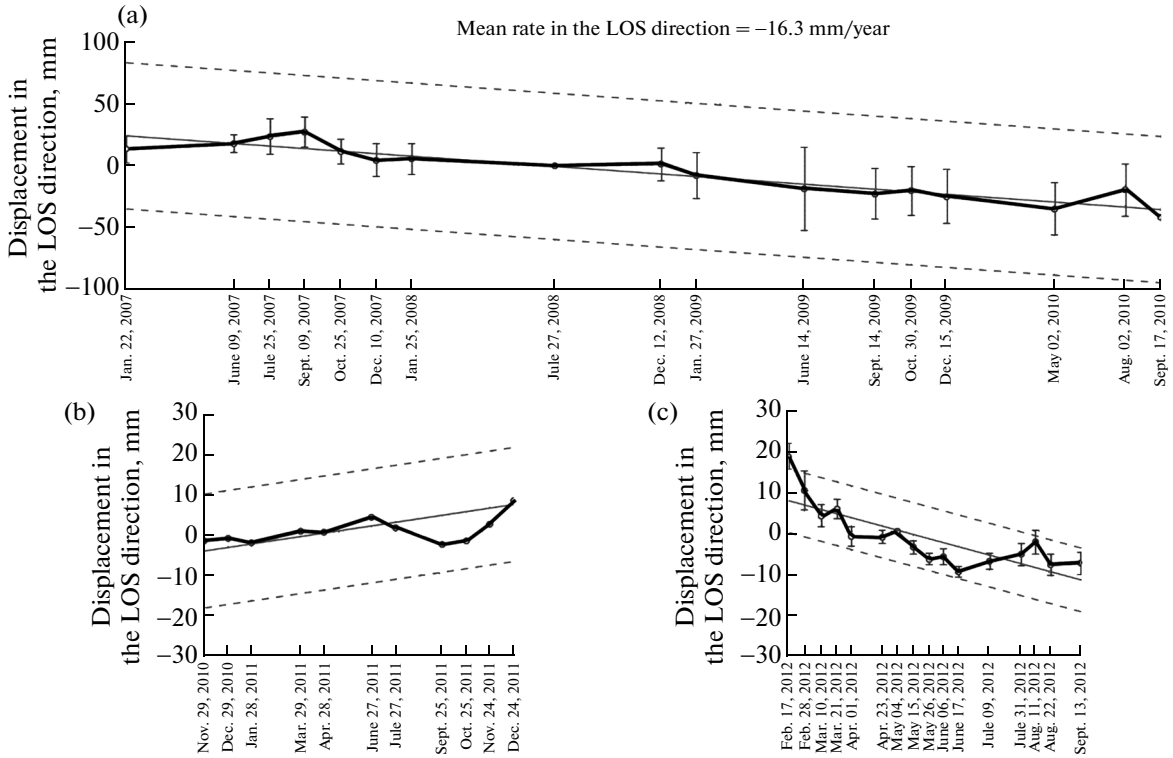

Fig. 5. The time series of displacements in the LOS direction as obtained from ALOS (a), ENVISAT (b), and TerraSAR-X (c) images for the Baranovka Settlement area. ENVISAT images were made from the descending orbit, while ALOS and TerraSAR-X images were made from the ascending orbit (see the flight directions in Fig. 4); this is the reason that displacements in the LOS direction are of opposite signs.

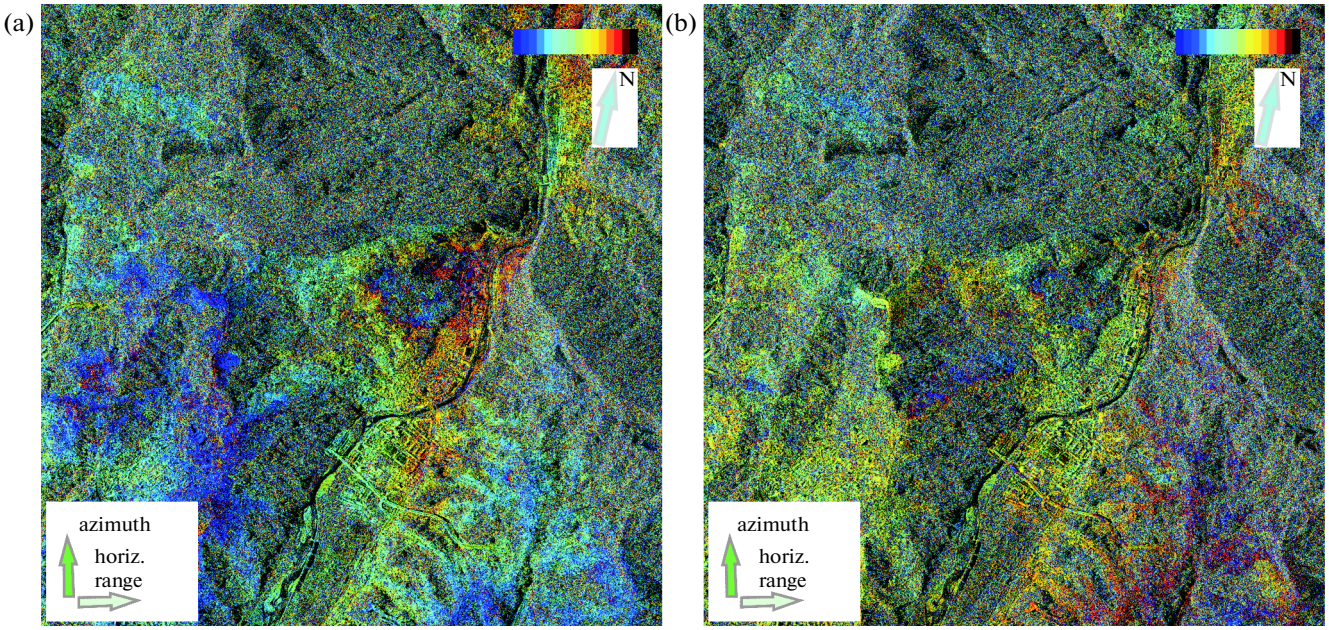

Fig. 6. Differential interferograms in radar coordinates for the landslide area in Baranovka Settlement, after the elevation effect is eliminated, as constructed from TerraSAR-X images of February 17–28, 2012 (a) and February 28–March 21, 2012 (b). The full color cycle corresponds to a displacement of 15.5 mm.

tion we can clearly see seasonal accelerations of displacements away from the satellite (down the slope) in the autumn–winter, while deceleration occurred in the summer. The time series of displacements from ENVISAT images can be clearly subdivided into two time intervals: (a) November 29, 2010–July 27, 2011 and (b) September 25–December 24, 2011, with the mean values of v_{LOS} = 20–21 and 50 mm/yr, respectively. This indicates a considerable acceleration of landsliding process in Baranovka Settlement as early as autumn 2011 and verifies the statements of eyewitnesses.

Let us analyze the time series of displacements in the LOS direction from TerraSAR-X images from February 17 until September 13, 2012 (Fig. 5c) in more detail. The displacement rate v_{LOS} in the period of February 17–March 10, 2012 was up to 30 mm/month; it then decelerated to 2–3 mm/month from June 6, 2012. This considerable decrease in displacement rate was verified by the ground-based data. Finally, in order to estimate the displacements in the February 12–March 10, 2012 period, let us analyze two differential interferograms: February 17–28, 2012 (Fig. 6a) and February 28–March 21, 2012 (Fig. 6b). Their visual analysis allows us to estimate the displacement lengths in the LOS direction for the respective periods (February 17–28, 2012 and February 28–March 21, 2012) at 10–12 and 5–7 mm. The good agreement between these values and v_{LOS} obtained on the time series (Fig. 5c) is good evidence of the validity of the results.

CONCLUSIONS

We studied three sets of radar satellite images with different wavelengths using three methods of SAR data analysis. The offset-tracking method enabled us to estimate the displacements that were produced by the landslide in the night between January 23 and 24, 2012. The following are the displacement values for the areas that were most affected by the landslide: approximately 6.4 ± 1 m in the northern part of Chereshnevyi per.; approximately 7.5 ± 1 m in the northern part of Kombinatskii per.; and 5.1 ± 1 m in the central part of Armyanskaya ul., near its crossing with Chereshnevyi per. The offset-tracking method also allowed us to define the landslide contours, including those on forested slopes without buildings.

As revealed by ALOS satellite images that were made from January 22, 2007 until September 17, 2010, displacements before the landslide activation demonstrate seasonal acceleration in the direction away from the satellite (down the slope) in the autumn–winter period. The time series of displacements that were revealed from ENVISAT images shows two stages of landslide development before the active phase: (a) November 29, 2010–July 27, 2011, when the mean displacements in the LOS direction were relatively small (approximately 21 mm/yr)and (b) September 25–December 24, 2011, when the displacements accelerated to v_{LOS} = 50 mm/yr immediately before the onset of the active phase. This indicates a considerable acceleration of the landsliding as early as autumn 2011. The revealed characteristics of the landslide dynamics are verified by the land-based and eyewitness data.

The dynamics of the landslide after the catastrophic activation were studied using short-wave images from the TerraSAR-X satellite. The displacement rate v_{LOS} in the February 17–March 10, 2012 period was up to 30 mm/month; it then decelerated to 2–3 mm/month from June 6, 2012; this is also verified by the land-based data. Displacements in the same period were also estimated from differential interferograms that showed displacements of 10–12 and 5–7 mm in the LOS direction in the February 17–28, 2012 and February 28–March 21, 2012 periods, respectively. The displacements in the first and second period agree with the displacement rates given above from the time series of TerraSAR-X images (Fig. 5c).

This work shows the high efficiency of satellite radar interferometry during the monitoring of landslide processes in the Northern Caucasus region, where observations are complicated by the mountain relief and dense forest vegetation cover on slopes. Additionally, the reasonability of the combination of different methods in analyzing the amplitude and phase of radar images has been demonstrated.

ACKNOWLEDGMENTS

The ENVISAT images were provided by the European Space Agency in the framework of the CIP7991 project. The TerraSAR-X images were provided by the German Aerospace Center (Deutschen Zentrums fur Luft- und Raumfahrt, or DLR) in the framework of the LAN 1247 research project. The ALOS images were purchased from the Japanese Aerospace Exploration Agency (JAXA).

REFERENCES

1. V. S. Verba, L. B. Neronskii, I. G. Osipov, and V. E. Turuk, *Spaceborne Radar Earth-Viewing Systems*, Ed. by V. S. Verba, (Radiotekhnika, Moscow, 2010) [in Russian].
2. V. O. Mikhailov, A. N. Nazaryan, V. B. Smirnov, E. A. Kiseleva, S. A. Tikhotskii, E. I. Smolyaninova, E. P. Timoshkina, S. A. Polyakov, M. Diament, and N. Shapiro, Izv., Phys. Solid Earth **46**, 91 (2010).
3. V. O. Mikhailov, E. A. Kiseleva, E. I. Smol'yaninova, P. N. Dmitriev, V. I. Golubev, Yu. S. Isaev, K. A. Dorokhin, E. P. Timoshkina, and S. A. Khairetdinov, Izv., Phys. Solid Earth **50**, 576 (2014). doi: 10.1134/s1069351314040107
4. A. Ferrett, C. Prati, and F. Rocca, IEEE Trans. Geosci. Remote Sens. **39**, 8 (2001).
5. A. Hooper, P. Segall, and H. Zebker, J. Geophys. Res. **112**, 07407 (2007).

6. A. Hooper, K. Spaans, D. Bekaert, M. C. Cuenca, M. Ankan, and A. Oyen, *StaMPS/MTI Manual* (Delft Inst. Earth Obs. Space Syst., Delfit, 2010). http://radar.tudelft.nl/~ahooper/stamps/StaMPS_Manual_v3.2.pdf
7. V. O. Mikhailov, E. A. Kiseleva, E. I. Smol'yaninova, P. N. Dmitriev, Yu. A. Golubeva, Yu. S. Isaev, K. A. Dorokhin, E. P. Timoshkina, S. A. Khairetdinov, and V. I. Golubev, Geofiz. Issled. **14** (4), 5 (2013).
8. A. L. Gray, N. Short, K. E. Mattar, and K. C. Jezek, Can. J. Remote Sens. **27**, 193 (2001).
9. T. Strozzi, A. Luckman, and T. Murray, IEEE Trans. Geosci. Remote Sens. **40**, 2384 (2002).
10. H. Liu, J. Yu, Z. Zhao, and K. C. Jezek, Int. J. Remote Sens. **28**, 1217 (2007).
11. J. Neelmeijer, M. Motagh, and H.-U. Wetzel, Remote Sens., No. 6, 9239 (2014).
12. R. F. Hanssen, *Radar Interferometry Data Interpretation and Error Analysis* (Kluwer Academic, Dordrecht, 2000).
13. P. N. Dmitriev, V. I. Golubev, Yu. S. Isaev, E. A. Kiseleva, V. O. Mikhailov, and E. I. Smolyaninova, Sovrem. Probl. Distantsionnogo Zondirovaniya. Zemli Kosmosa **9** (2), 130 (2012).
14. N. K. Kononova, Slozhnye Sist., No. 2, 11 (2014).
15. https://rospravosudie/com/court-centralnyj-rajonnyj-sud-g-sochi-krasnodarskij-kraj-s/act-413232109/

Translated by N. Astafiev